Influence of defect density states on NO2 gas sensing performance of Na: ZnO thin films

Article *in* Journal of Sol-Gel Science and Technology · June 2023

DOI: 10.1007/s10971-023-06155-1

Journal of Sol-Gel Science and Technology
https://doi.org/10.1007/s10971-023-06155-1

ORIGINAL PAPER: SOL-GEL AND HYBRID MATERIALS FOR CATALYTIC, PHOTOELECTROCHEMICAL AND SENSOR APPLICATIONS

Influence of defect density states on NO_2 gas sensing performance of Na: ZnO thin films

K. K. Jasmi[1] · T. Anto Johny[1] · V. S. Siril[2] · K. N. Madhusoodanan[2]

Received: 31 March 2023 / Accepted: 31 May 2023

Abstract

In this work, the $Zn_{1-x}Na_xO$ (x = 0, 0.01, 0.03, and 0.05) thin film gas sensors were prepared via the sol-gel spin coating method to study the impact of sodium on structural, morphological, elemental, electrical, and gas sensing applications. Crystal structure (XRD), energy dispersive X-ray analysis (EDX), X-ray photoelectron spectroscopy (XPS), field emission scanning electron microscopy (FESEM), four-probe hall measurement, and NO_2 gas sensing properties were investigated to ascertain the elemental composition, morphology, defect density states, working temperature, response/recovery time, stability, selectivity, and repeatability. The 3 wt.%Na:ZnO gas sensor displays a gas-accessible structure with more oxygen vacancies, remarkable stability, and sensitivity towards NO_2 gas at an optimum temperature (210 °C). A possible gas-sensing mechanism was also discussed and correlated with structural, elemental, morphological, and electrical properties.

Graphical Abstract

Pure, 1 wt.% Na-doped, 3 wt.% Na-doped, and 5 wt.% Na-doped ZnO thin film sensors were fabricated via the sol-gel spin coating technique and exhibited a hexagonal wurtzite structure. The incorporation of Na into the ZnO matrix was confirmed by EDX and XPS analysis. The 3%Na-doped ZnO thin film exhibits more oxygen vacancies and carrier concentration. The 3%Na-doped ZnO thin film shows an enhanced gas sensing response of 22.53 against 75 ppm of NO_2 gas. Good selectivity, outstanding stability, rapid response and recovery times, and excellent reproducibility are all demonstrated by the 3%Na-doped ZnO.

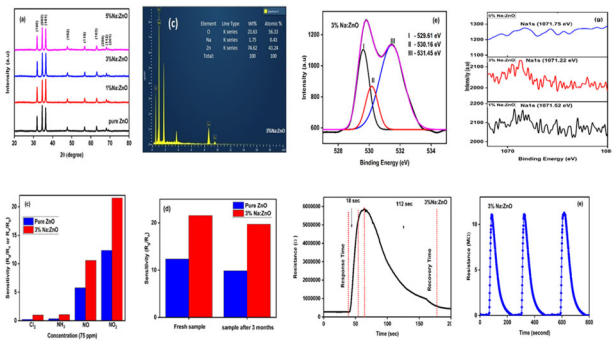

Keywords Na:ZnO · porous structure · NO_2 Gas sensing · Crystal defect · stability · selectivity

✉ K. K. Jasmi
jasmifirdhouse@gmail.com

[1] Department of Physics, St. Thomas' College, Affiliated to University of Calicut, Thrissur 680001, India

[2] Department of Instrumentation, Cochin University of Science and Technology, Cochin 682022, India

Published online: 14 June 2023

Highlights

- Through sol-gel spin coating technique, pure, (1,3, and 5) wt.% Na-doped ZnO thin film sensors were fabricated and characterized.
- 3 wt.%Na-doped ZnO thin film with porous structure exhibit more oxygen vacancies and carrier density.
- 3%Na-doped ZnO thin film shows enhanced gas sensing performance against 75 ppm of NO_2 gas.

1 Introduction

Nowadays, industrialization and urbanization release a wide range of harmful gases into the atmosphere, including H_2S, CO_2, NH_3, NO_2, Cl_2, etc., which harm human health and the environment. Amongst, nitrogen dioxide (NO_2), a major air pollutant, is produced by burning fossil fuels, leading to acid rain and can cause lung and respiratory-related diseases [1]. So there is a greater need to develop NO_2 gas sensors with low optimal temperatures, remarkable gas sensitivity, outstanding stability, and excellent repeatability. Recently, several research groups have focused on developing metal oxide semiconductor (MOS) gas sensors, such as Fe_2O_3, CuO, NiO, In_2O_3, WO_3, SnO_2, ZnO, Co_3O_4, etc., to detect oxidizing and reducing gases [2–9].

Among the assorted MOS gas sensors, Zinc Oxide (ZnO) is attracted by many researchers due to its exceptional features such as broad bandgap, high exciton binding energy, a wide range of electrical resistivity from 10^4 to 10^{12} Ω-cm, abundance in nature, nontoxicity, environmental friendliness, suitable for doping, etc. [10]. Even though ZnO is a promising candidate for monitoring various toxic gases like CH_4, NH_3, Cl_2, NO_2, H_2S, CO, etc. In addition, ZnO has numerous drawbacks, including low reliability, low gas sensitivity, and a high working temperature, which may restrict its gas-sensing applicability [11–14]. Novel methods of ZnO fabrication and doping with relevant elements have been used to address these limitations of ZnO gas sensors.

Many research groups have focused to developed porous, nanocomposite, nano-rod, nano-strutured, hetero-structured, and utilizing suitable dopants to enhance the gas sensing efficiency of ZnO [15–20]. However, little attention is paid to doping ZnO with alkali metals (Li, Na, or K) to improve gas sensitivity [10, 21, 22]. Our earlier published work demonstrates that Li-doped ZnO successfully improves NO2 gas detection [23]. For improved NO_2 gas sensing applications, we here further develop another alkali metal (Na)-doped ZnO. Sodium (Na) is one of the appropriate materials which can tailor the structural, morphological, elemental, and gas-sensing properties of ZnO. The ionic radius of sodium (95 pm) is higher as compared with zinc (74 pm), which may substitute either an interstitial site of ZnO (Na_i) or a lattice site of ZnO (Na_{Zn}), expecting n-type conductivity or p-type conductivity, respectively [24, 25]. It has a shallow substitutional level, expected to be 170 meV below the conduction band minimum (CBM) [11, 12, 25]. The strength of interaction between the defect density states, formed by Na doping, and the inherent defect states might play a prominent role in the electrical characteristics and gas sensing capabilities of Na:ZnO [24, 26–31]. When Na is substituted, the defect states may align closely with the inherent defect states of ZnO, leads to enhance NO_2 gas sensitivity. Thus, alkali metal-doped ZnO was considered to be a promising material for device applications for future study.

In this scenario, we have prepared Na (0, 1, 3, and 5 wt.%) doped ZnO (Na: ZnO) thin films via the sol-gel spin-coating technique for NO_2 gas sensing applications. The deposited thin film samples were examined through various characterization techniques, including XRD, XPS, FE-SEM, EDX, and the Hall measurements to investigate the effect of Na on the structural, morphological, and electrical properties of Na: ZnO thin-film. Among the deposited samples, 3%Na:ZnO thin film sensor exhibits the remarkable sensitivity and rapid response/ recovery duration toward NO_2 gas at its optimum temperature of 210°C. Also, a possible the gas sensing mechanism was discussed and correlates it with defect density states of Na: ZnO.

2 Experimental techniques

2.1 Chemical reagents

All chemical reagents used ACS-quality that can be used without further purification., zinc acetate dehydrate ($Zn(CH_3COO)_2.2H_2O$), sodium acetate trihydrate ($CH_3COONa{\cdot}3H_2O$), diethanolamine (DEA), and isopropyl alcohol (IPA), are purchased from Sigma Aldrich (India). Calibrated Nitrogen dioxide (NO_2) gas cylinders purchased from Chemtron scientific laboratory, Pvt. Ltd, India.

2.2 Film fabrication

The Na:ZnO thin-film gas sensors were fabricated via sol-gel spin coating on a low-cost, transparent, heat-resistive glass substrate [26–28]. To ensure the quality of the deposited films, the substrate was first cleaned with an ultrasonic cleaner followed by acetone. We prepared the precursor solution of 0.5 M by adding equimolar amounts of DMA (stabilizer) and the required quantity of zinc acetate dihydrate to the IPA (solvent). The mixture was then stirred

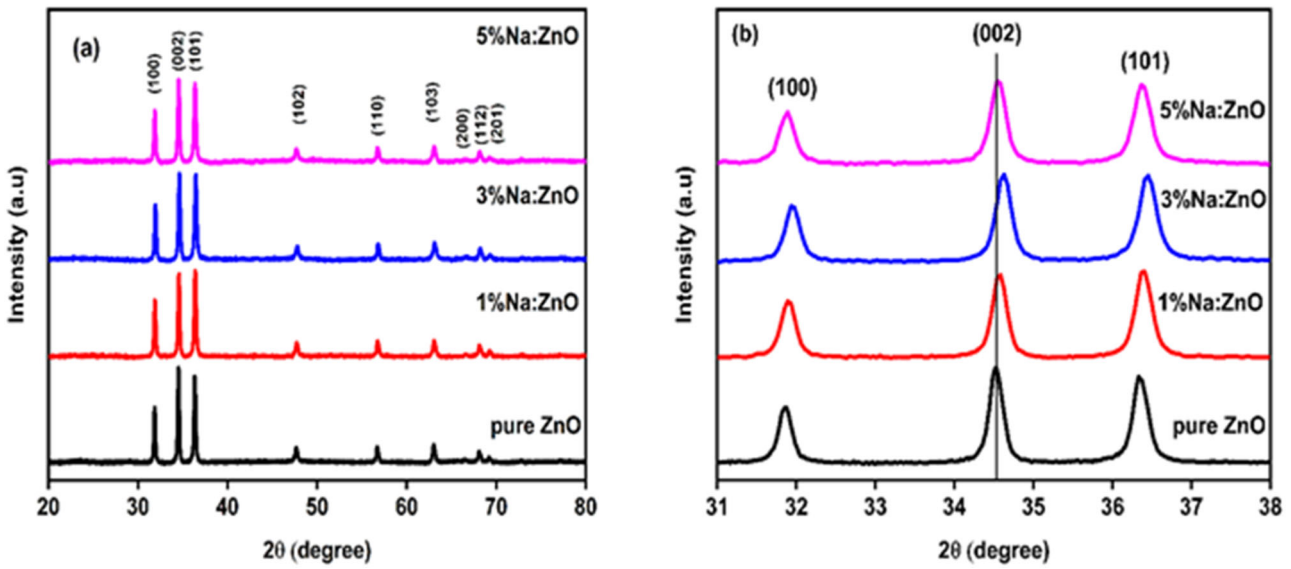

Fig. 1 **a** X-ray diffraction spectra and (**b**) zoomed XRD spectra of Na:ZnO thin film sensor

at room temperature until a clear solution was obtained. Then, add the necessary amount of sodium acetate trihydrate (0, 1, 3, and 5 wt.%) and stir until the solution turns transparent. For stability, we stored the prepared solution for 48 h before spin-coating it onto a glass substrate and drying it at 150 °C in a hot air oven for 20 min, followed by 30 min of annealing at 500 °C in a tube furnace as per our previous fabrication procedure [23, 32].

2.3 Thin films characterization

The crystalline structure studies were carried out by X-ray diffractometer (PAN Analytical, Japan, $\lambda = 0.154$ nm with Cu-Kα radiation), surface morphology and elemental composition collected from FESEM Carl Zeiss Supra, 40 VP, EDX (Joel, JSM-6010), and chemical state of elements obtained from XPS (Kraton, Axis Ultra). Electrical parameters of the thin films were measured at RT by a four-probe Hall measurement system, HMS-3000, Ecopia, S. Korea. The gas sensing parameters of the Na:ZnO thin-film sensors were collected from a Keysight 34461 A (6.5-resolution) multimeter while it was exposed to different concentrations of NO_2 gas at optimal temperature (210 °C). Finally, to ensure a moisture-free environment and for baseline resistance stabilization, the gas sensors were pre-heated for 20 min at 500 °C and humidity had been negligible at high temperatures above 150 °C [33]. Sensitivity is defined as follows [34]:

$$\text{For an oxidizing gas, sensitivity} = \frac{R_{gas}}{R_{air}},$$

$$\text{And for reducing gas, sensitivity} = \frac{R_{air}}{R_{gas}}$$

Table 1 XRD parameters of Na:ZnO thin films

Thin films	FWHM(β) (deg)	Lattice parameters (Å) a = b	c	Crystallite size (D) (nm)	Volume (Å)^3
Pure ZnO	0.4853	2.8804	4.983	16.37	35.79
1%Na:ZnO	0.4473	2.8571	4.9427	17.76	34.94
3%Na:ZnO	0.3471	2.8604	4.9484	22.89	35.06
5%Na:ZnO	0.3749	2.8542	4.9377	21.19	34.83

3 Result and discussions

3.1 structural study

Figure 1a depicts the XRD pattern of Na:ZnO thin films (0, 1, 3, and 5 wt.%). All the obtained peaks are attributed to the hcp structure of ZnO according to JCPDS card No-89-0510 with no extra diffracted peaks observed corresponding to Na or Na_2O [35]. In the ZnO lattice, Na atoms are either replaced by Zn atoms (Zn_{Na}) or introduced into interstitial sites (Na_i). The peaks are slightly shifted to the higher angle side up to 3% Na:ZnO, after which they tend to shift towards the lower angle side. This suggests that up to 3% Na: ZnO, Na enters the interstitial site rather than the lattice site, after which Na occupies the lattice site instead of an interstitial site, Fig. 1b [23, 36–39]. Na interstitials are present close to oxygen vacancies (VO), which is favorable for improved gas sensitivity [40]. The crystal structure of ZnO is not altered by doping sodium, but it affects the peak intensity. In order to investigate the causes of this reduction in intensity, various

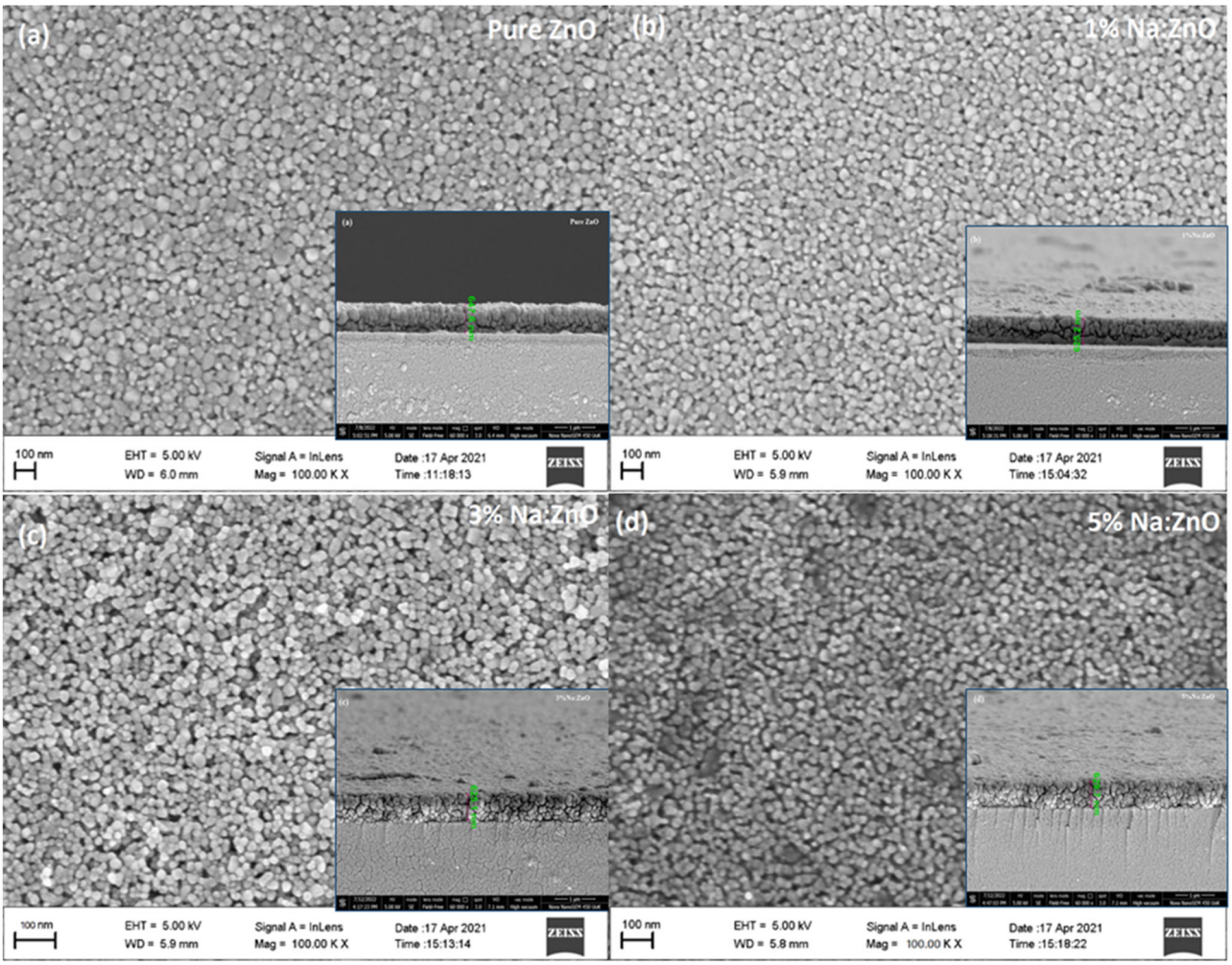

Fig. 2 FE-SEM (surface and cross sectional) image of (**a**) pure ZnO, (**b**) 1%Na:ZnO, (**c**) 3%Na:ZnO and (**d**) 5%Na:ZnO thin film sensor

lattice parameters are determined. The following equations are used to compute the lattice constants "a", "c", volume (V) and crystallite size (D) of ZnO thin films with (002) orientations: $a = \frac{\lambda}{\sqrt{3}\sin\theta}$, $c = \frac{\lambda}{\sin\theta}$, $V = \frac{\sqrt{3}a^2c}{2} = 0.866a^2c$ and Scherrer's equation $D = \frac{0.9\lambda}{\beta\cos\theta}$. Where θ is the Bragg's angle, λ is the X-ray wavelength, and β is the full width at half maximum (FWHM) of the (002) plane. Table 1 shows the lattice parameters a, c, crystallite size, volume, and FWHM along the (002) plane. It shows FWHM decreases, but crystallite size shows an increasing trend with Na doping and a decrease after 3% Na:ZnO, reveals that dopants can act as nucleation sites, promoting crystallite formation [41]. Na has essentially no impact on the ZnO host since there is only a small change in the lattice parameter of ZnO.

3.2 FE-SEM analysis

The morphology of the ZnO nanostructures changed by Na doping is identified using FE-SEM analysis, as shown in Fig. 2a–d and the histogram is used to determine the grain size of Na:ZnO, depicted as Fig. 3. In 1%Na:ZnO, the surface morphology changes significantly, and the grain size reduces when compared to pure ZnO, Figs. (2b, 3b). The decrease in trend in grain size has continued up to 3% Na:ZnO with larger voids and a porous structure, serving as an active site for the test gas, Figs. (2c, 3c). It is due to insoluble Na atoms being segregated at the grain boundaries and that leads to suppression of ZnO crystal growth at the same time it can act as nucleation sites, promoting crystallite formation, Table 1 [35, 42, 43]. Besides, in 5% Na:ZnO, particles accumulate more and exhibit a high degree of aggregation, Figs. (2d, 3d). The fluctuation in surface energy due to the local inhomogeneity of sodium distribution may be the cause this alteration. A cross-sectional section image of FE-SEM (insert of Fig. 2a–d) is employed to compute the thickness of a Na:ZnO thin film sensor, with a range of 625–648 nm (inset of Fig. 2a–d) [44, 45]. The elemental distribution of the pure and Na:ZnO samples is confirmed by EDX analysis and is displayed in

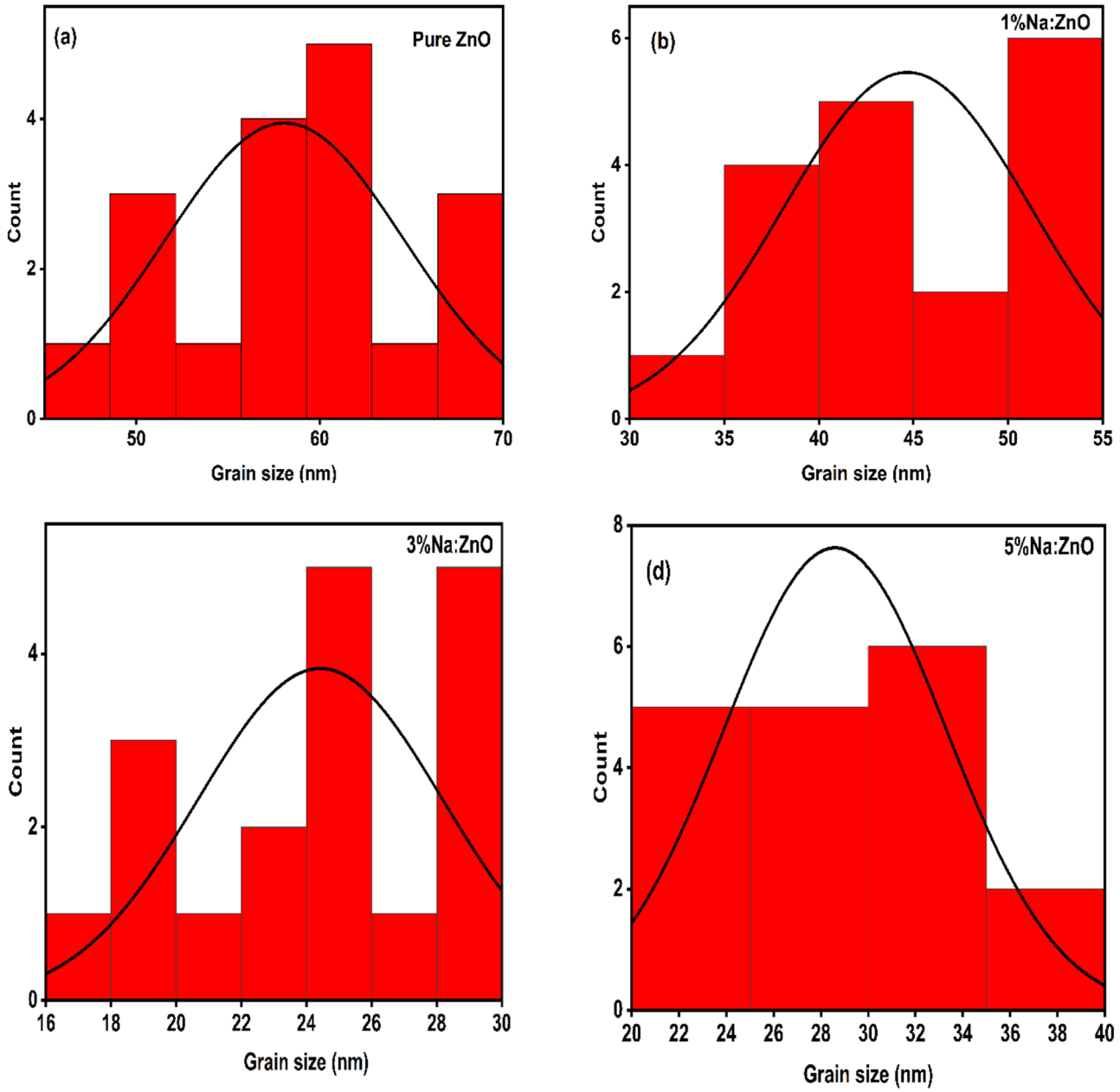

Fig. 3 Size distribution histogram diagram of Na:ZnO thin film sensor

Fig. 4a–d. The EDX results reveal that Zn and O are present in pure ZnO, instead Na, Zn, and O were seen in Na-doped ZnO thin films, which gives clear evidence that Na was successfully doped into the ZnO matrix.

3.3 Hall measurement

The electrical conductivity studies of Na:ZnO thin-films have been evaluated using a four-probe Hall measurement system, and the results are tabulated in Table 2. The electrical conductivity measurement reveals that pure, 1, and 3 wt% Na:ZnO thin film sensors exhibited n-type, whereas 5 wt% Na:ZnO is p-type. Usually, oxygen vacancies of ZnO are of shallow donor levels just below the conduction band minimum (CBM) for the *n*-type ZnO, (Table 2a) this may be expressed using the Kroger-Vink notation, Eq. (1) [32].

$$ZnO \Leftrightarrow Zn_{Zn}^{x} + \dot{V}_{o} + e' \quad (1)$$

In both the 1%Na:ZnO and 3%Na:ZnO thin film sensors, Na is expected to occupy the interstitial site and release an electron for conduction. As a result, electrical resistance

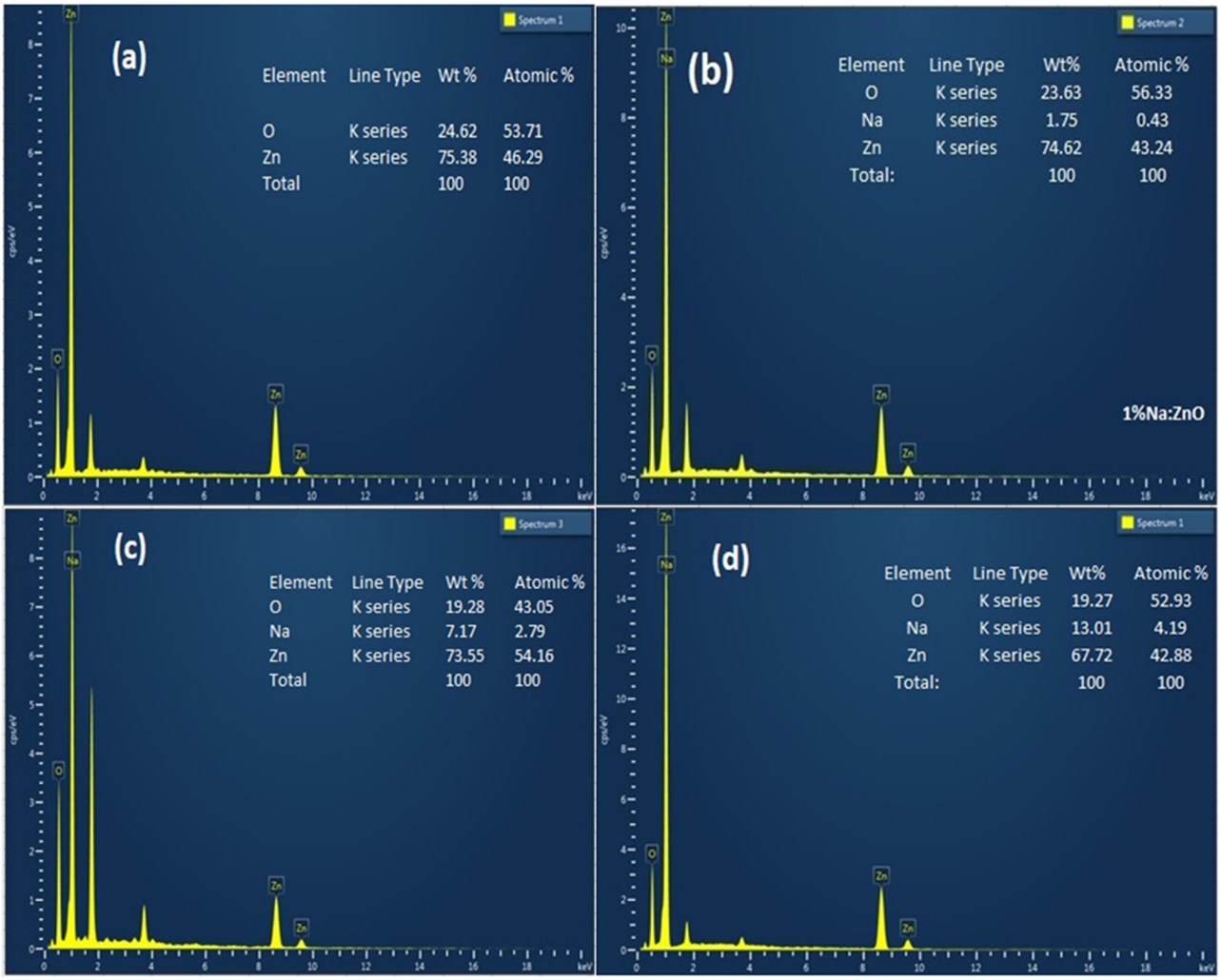

Fig. 4 EDX image of (**a**) Pure, (**b**) 1%Na:ZnO, (**c**) 3%Na:ZnO, and (**d**) 5%Na:ZnO thin film sensor

Table 2 Gas-sensing and electrical parameters of Na:ZnO thin-films

Thin Film	Carrier-concentration (per cm^3)	Resistivity (Ω-cm)	Mobility (cm^2/Vs)	Type	Gas-Sensitivity (R_g/R_a)	Response/ Recovery Time (s)
(a) Pure ZnO	1.16×10^{15}	1.17×10^{3}	4.63	*n*	12.35	22/193
(b) 1%Na: ZnO	1.41×10^{16}	2.34×10^{2}	1.9	*n*	17.94	16/141
(c) 3%Na: ZnO	2.09×10^{16}	7.46×10^{1}	4.01	*n*	21.53	18/112
(d) 5%Na: ZnO	2.68×10^{14}	1.03×10^{3}	22.58	*p*	17.23	18/146

decreases with increasing carrier concentration, as expressed in Eq. (2), (Table 2b, c).

$$Na_2O \overset{2ZnO}{\Leftrightarrow} \dot{Na}_i + e' + O_O^x \tag{2}$$

Besides 5%Na:ZnO, shows p-type conductivity with a significant increase in resistance and a reduction in carrier concentration, as per Eq. (3), (Table 2d) [24].

$$Na_2O \overset{2ZnO}{\Leftrightarrow} 2Na'_{Zn} + O_0^x + 2\dot{h} \tag{3}$$

3.4 XPS analysis

The extended effect of defect states in Na:ZnO thin films has been investigated using XPS. We have also attempted to correlate the roles of Na ions that are either interstitial (Na_i) or substitutional (Na_{Zn}) in the presence of oxygen vacancy defects. There are several distinct peaks seen that are caused by absorbed carbon, Zn, O, and Na. However, there are no peaks associated with impurity components within the

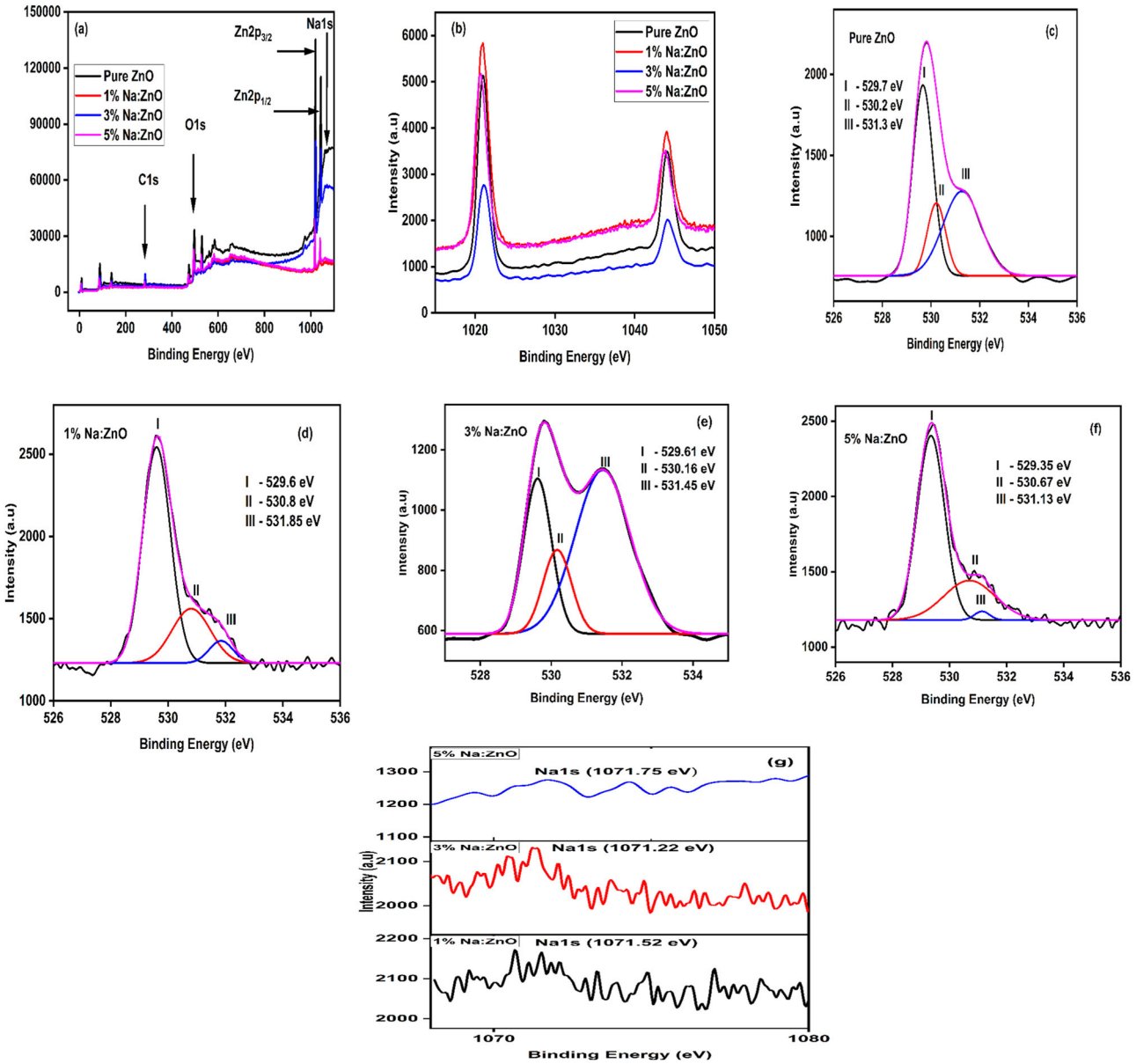

Fig. 5 **a** XPS survey study, (**b**) Scan for Zn2p spectra, (**c–f**) spectra of O 1 s and (**g**) Na 1 s binding energy level

detection limit. The XPS survey spectra of the Na:ZnO thin film are shown in Fig. 5a. High-resolution XPS spectra of Zn, Na, and O have been collected to evaluate the influence of Na on ZnO samples. Figure 5(b) reveals that the binding energies of Zn $2p_{3/2}$ and $2p_{1/2}$; the energies between the two states, which correspond to pure 1%Na:ZnO, 3%Na:ZnO, and 5%Na:ZnO thin films, are 23.1 eV, 23.05 eV, 23 eV, and 23.1 eV, respectively, concurring with previous reports [46].

The oxygen vacancies of Na:ZnO thin film samples has been calculated by fitting the O 1 s peak into three peaks (I, II, and III) using Gaussian multiple peaks fit, as depicted in Fig. 5c–f. Peak I is attributed to O_2 surrounded by ZnO crystals, peak II to lack oxygen in ZnO compound, and peak III to oxygen-deficient Zones. The results revels that, 3% Na:ZnO thin film sensor, as displayed in Table 3, has significantly greater oxygen vacancies, making it a suitable choice for NO_2 gas sensing applications. Additionally, XPS Na 1 s spectra reveal that the 3% Na:ZnO thin film sensor has

Table 3 Oxygen defects among the deposited samples

Thin film	Peak I	Peak II	Peak III
Pure ZnO	45.9%	38.1%	16%
1%Na:ZnO	59.7%	24.1%	26.2%
3%Na:ZnO	27.4%	15.2%	57.4%
5%Na:ZnO	74.2%	6.3%	19.5%

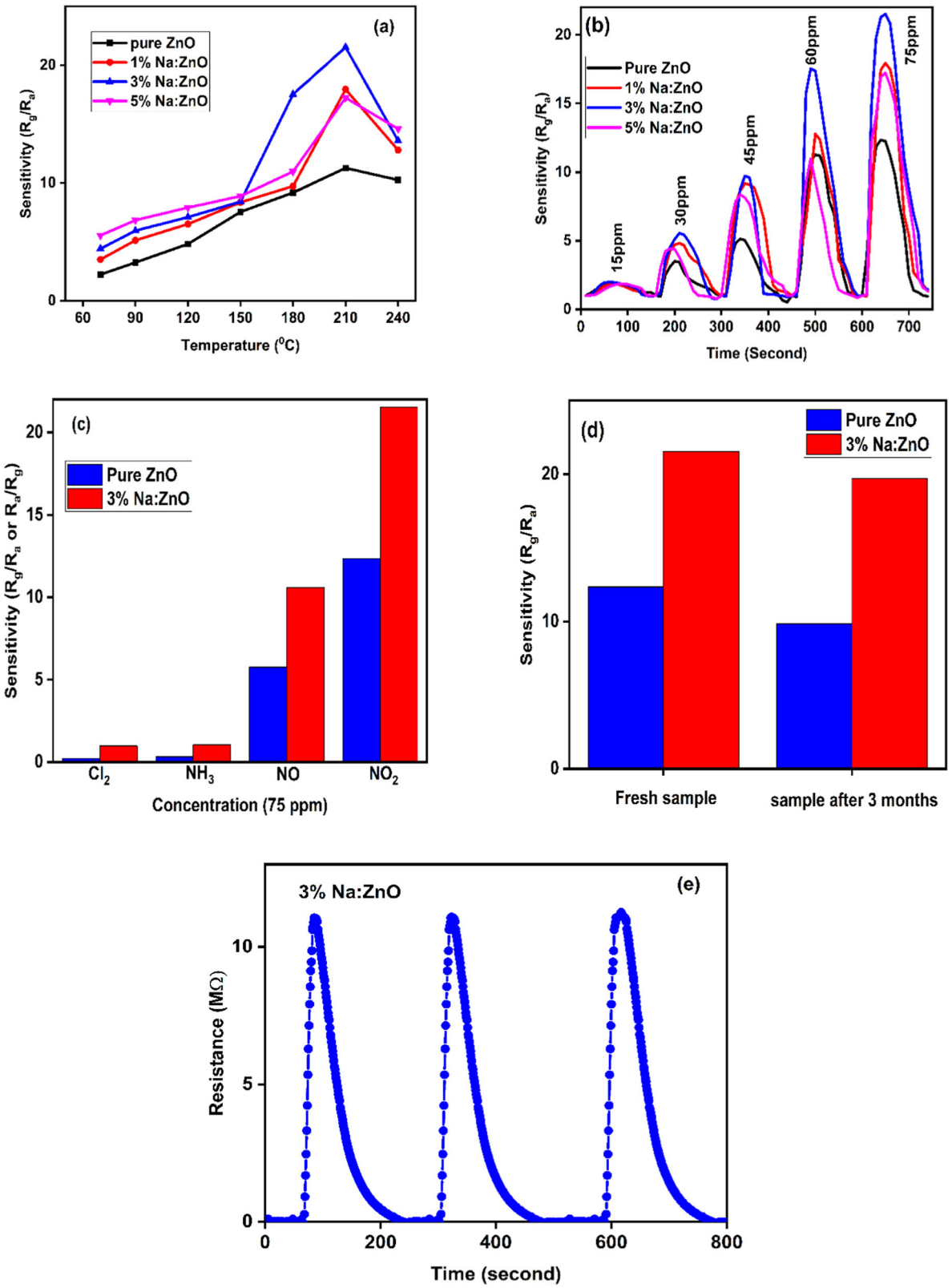

Fig. 6 **a** Sensitivity-Temperature plot, (**b**) Dynamic Response-time graph, (**c**) Selectivity of pure and 3%Na:ZnO towards various gas, (**d**) Stability measure of pure and 3%Na:ZnO thin films and (**e**) Reproducibility of 3%Na:ZnO thin-film sensor towards 75ppm NO_2 gas

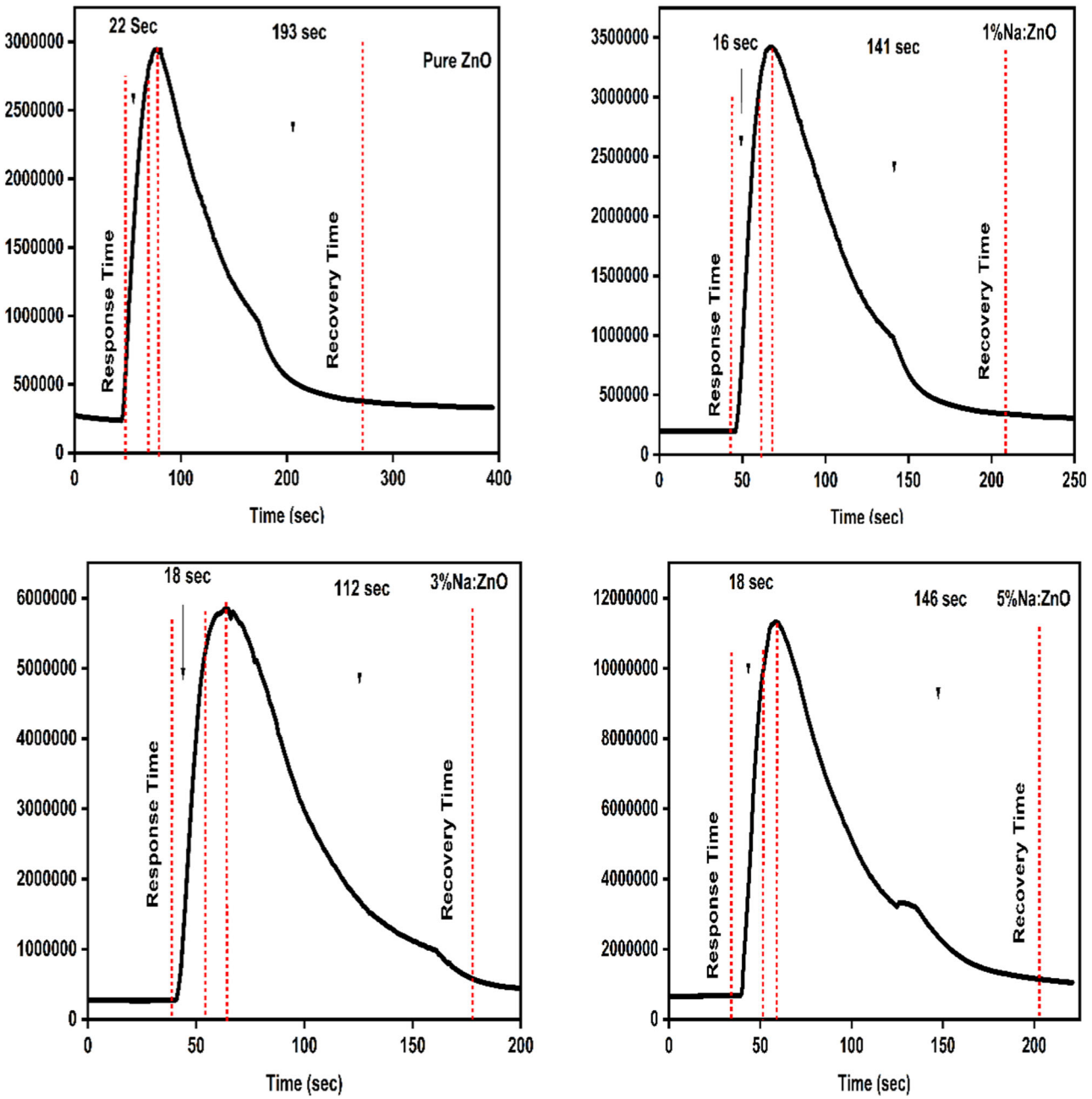

Fig. 7 Resistance-time graph of Na:ZnO thin films

a lower binding energy (1071.22 eV), confirming the interstitial substitution of Na^{+} (Na_i), while the 5% Na: ZnO thin film sensor has a higher binding energy (1071.75 eV), confirming the lattice substitution (Na_{zn}) in the ZnO matrix [30].

3.5 Gas sensing study

The sensitivity of a MOS gas sensor mostly depends on the optimal temperature. In this study, primarily, gas sensing performance of the fabricated samples were tested at various temperatures (70–240 °C) after being exposed to 75ppm of NO_2 gas Fig. 6a [23]. Further, the gas-sensing studies of the pure and Na:ZnO thin-film sensors with various NO_2 gas concentrations (15ppm to 75ppm) are studied, Fig. 6b. Besides, the response/recovery duration and NO_2 gas sensitivity of Na:ZnO thin film sensors at 75ppm are measured, Fig. 7 and Table 2. In short, the optimum temperature and suitable material for gas sensing applications are 210 °C and 3% Na:ZnO, respectively.

As part of the selectivity study, pure and 3%Na:ZnO thin films were exposed to 75ppm of various toxic gases (Cl_2, NH_3, NO and NO_2) at 210 °C, and the results showed

Table 4 Comparison of different dopants on ZnO thin films for NO_2 gas sensing performance

Sl. No	Dopant	Optimum temperature (^{0}C)	Sensitivity	Response time/ Recovery time (s)	Bibliography
1	ZnO-branched SnO_2 nanowires	300	26.61	550/100	[50]
2	Ga_2O_3-core/ZnO-shell	300	7246.6%	840/400	[51]
4	Nb/ZnO	300	1640%	30/250	[52]
5	ZnO/CuO NWs	350	30	250/340	[53]
6	ZnO-decorated MWCNT	300	1.023	93.1/285.2	[54]
7	Al/ZnO	250	11	540/ 600	[55]
8	Na:ZnO	210	21.53	18/112	Present study

our samples were most selective to the NO_2 gas, (Fig. 6c). Then, the gas sensing measurements of pure and 3% Na:ZnO sensors were performed at 210 °C, in the presence of 75 ppm of NO_2, in order to depicts their long-term durability. For freshly prepared samples, gas sensitivity was determined to be 12.35 and 21.53, respectively. Additionally, the gas sensing measurement has been performed after three months, with 9.86 (decreased by 20.3%), and 19.7 (decreased by 8.4%), demonstrates the superior quality of 3%Na:ZnO thin film, Fig. 6d. Also, the reproducibility of 3%Na:ZnO thin films was tested, and results show that sensor behavior does not significantly change, (Fig. 6e). In summary, 3%Na:ZnO is a desirable material for gas sensing devices. In Table 4, we summarize the comparative study of different dopants on ZnO thin films for NO_2 gas sensing.

3.6 Gas sensing mechanism

The gas sensing mechanism of MOSs mostly depends on the change in resistance in the presence of the test gas, by the formation of free electrons at the surface of ZnO. Oxygen vacancies and sensor resistance are improved when the dopant is incorporated. The oxygen vacancies play a key role in gas sensing mechanism [34]. In this study, 3% Na:ZnO thin film sensor have more surface oxygen vacancies as proved by XPS result (Fig. 5e), and Table 3. Thus, oxygen vacancy plays a key role on gas sensing mechanism, the oxygen vacancy defects are more favored for adsorption site of NO_2 gas, this could be explained using the following Eqs. (4) and (5) [38, 39].

$$Zn_xO_{x-1} + O_V + e^- + NO_2 \rightarrow ZnO + NO_{(ads)} \quad (4)$$

$$No_{(ads)} + ZnO \rightarrow NO + ZnO \quad (5)$$

At room temperature, the oxygen ion adsorbed on the surface of the thin film sensor withdraw electrons from the conduction band, resulting in negatively charged species [23, 47, 48]. When NO_2 gas is introduced, it interacts with the previously adsorbed O^{2-} as shown in the equation below (6) [49].

$$NO_{2(ads)} + O^{2-}_{(ads)} + 2e^- \Leftrightarrow NO^-_{2(ads)} + 2O^-_{(ads)} \quad (6)$$

As a result, a potential barrier is formed with a positive charge in the semiconductor and a negative charge on the adsorbed gases. In the presence of NO_2 gas, the height of the barriers enlarges due to the withdrawal of extra electrons from the surface of thin film sensor, resulting in an increase in sensor resistance. This could be explained by Na has a shallow substitutional level, just below CBM, closely associated with oxygen vacancy. As a result, the interaction between the defect states created by the dopant and the intrinsic defects of ZnO becomes prominent leads to remarkable gas sensitivity, Fig. 6b. The sharp increase in sensitivity also may be due to a decrease in grain size with porous and voids structure, as shown in Fig. 2c, also provides active site for NO_2 gas adsorption. Meanwhile, it can be concluded that, the 3%Na:ZnO shows remarkable NO_2 gas sensing performance and rapid response/recovery time were suitable for device application.

4 Conclusion

In this study, pure/Na:ZnO thin film gas sensors are fabricated for NO_2 gas sensing applications via the sol-gel spin coating technique. The influence of Na dopant to the structural, morphological, and electrical features of the ZnO samples are analyzed via XRD, XPS, FE-SEM, EDX, and a four-probe Hall measurement system. The hexagonal wurtzite phase of the prepared samples is verified by XRD data. Spherical and irregular particles with average grain sizes ranging from 24 to 58 nm with Na substitution and thicknesses ranging from 625 to 648 nm have been revealed by FE-SEM analysis. Four-probe Hall measurement provides the electrical conductivity, and the XPS spectra prove the existence of defect states in Na:ZnO thin film sensors. The low resistive 3%Na:ZnO

displays a gas-accessible structure with more oxygen vacancies showed remarkable stability and sensitivity toward NO_2 gas. Therefore, our research affirms that the 3%Na:ZnO is one of the best combination to tune the density of defect states host system and is a promising material for future gas sensing applications.

Compliance with ethical standards

Conflict of interest The authors declare no competing interests.

References

1. Sun N, Tian Q, Bian W, Wang X, Dou H, Li C (2023) Highly sensitive and lower detection-limit NO_2 gas sensor based on Rh-doped ZnO nanofibers prepared by electrospinning. Appl Surf Sci 614. https://doi.org/10.1016/j.apsusc.2022.156213.
2. Wang X, Wang T, Si G, Li Y, Zhang S, Deng X, et al. (2020) Oxygen vacancy defects engineering on Ce-doped α -Fe_2O_3 gas sensor for reducing gases. Sensors Actuators B. Chem 302. https://doi.org/10.1016/j.snb.2019.127165.
3. Diao K, Xiao J, Zheng Z, Cui X (2018) Enhanced sensing performance and mechanism of CuO nanoparticle-loaded ZnO nanowires: Comparison with ZnO-CuO core-shell nanowires. Appl Surf Sci 459 https://doi.org/10.1016/j.apsusc.2018.07.112.
4. Nakate UT, Ahmad R, Patil P, Yu YT, Hahn Y (2020) Ultra thin NiO nanosheets for high performance hydrogen gas sensor device. Appl Surf Sci 506. https://doi.org/10.1016/j.apsusc.2019.144971.
5. Han D, Zhai L, Gu F, Wang Z (2018) Highly sensitive NO_2 gas sensor of ppb-level detection based on In_2O_3 nanobricks at low temperature. Sensors Actuators B Chem 262. https://doi.org/10.1016/j.snb.2018.02.052.
6. Wang M, Wang Y, Li X, Ge C, Hussain S, Liu G (2020) WO_3 porous nanosheet arrays with enhanced low temperature NO_2 gas sensing performance. Sensors Actuators B Chem 316. https://doi.org/10.1016/j.snb.2020.128050.
7. Wu P, Li Y, Xiao S, Chen J, Tang J, Chen D, Zhang X (2022) SnO_2 nanoparticles based highly sensitive gas sensor for detection of C 4 F 7 N: a new eco-friendly gas insulating medium. J Hazard. Mater 422. https://doi.org/10.1016/j.jhazmat.2021.126882.
8. Suganthi K, Vinoth E, Sudha L, Bharathi P, Navaneethan M (2023) Manganese (Mn^{2+}) doped hexagonal prismatic zinc oxide (ZnO) nanostructures for chemiresistive NO_2 sensor. Sensors Actuators B 380. https://doi.org/10.1016/j.snb.2023.133293.
9. Hsueh T, Wu S (2021) Highly sensitive Co_3O_4 nanoparticles/MEMS NO_2 gas sensor with the adsorption of the Au nanoparticles Sensors Actuators B Chem 329. https://doi.org/10.1016/j.snb.2020.129201.
10. Basyooni MA, Shaban M, El Sayed AM (2017) Enhanced Gas Sensing Properties of Spin-coated Na-doped ZnO Nanostructured Films. Nat Publ Gr 7. https://doi.org/10.1038/srep41716.
11. Punia K, Lal G, Dolia SN, Kumar S (2020) Defects and Oxygen vacancies tailored structural, optical, photoluminescence and magnetic properties of Li doped ZnO nanohexagons. Ceram Int 46 https://doi.org/10.1016/j.ceramint.2020.01.280.
12. Lü J, Huang K, Chen X, Zhu J, Meng F, Song X, Sun Z (2011) Enhanced photo-induced hydrophilicity of the sol-gel-derived ZnO thin films by Na-doping. Appl Surf Sci 257. https://doi.org/10.1016/j.apsusc.2010.09.054.
13. Park CH, Zhang SB, Wei SH (2002) Origin of p-type doping difficulty in ZnO: The impurity perspective. Phys Rev B—Condens Matter Mater Phys 66. https://doi.org/10.1103/PhysRevB.66.073202.
14. Agrawal J, Dixit T, Palani IA, Rao MSR, Singh V (2018) Fabrication of high responsivity deep UV photo-detector based on Na doped ZnO nanocolumns, J Phys D Appl Phys 51. https://doi.org/10.1088/1361-6463/aab8d3.
15. Sharma B, Sharma A, Joshi M, Myung J (2020) Sputtered SnO_2/ZnO Heterostructures for Improved NO_2 Gas sensing properties. Chemosensors, 8. https://doi.org/10.3390/chemosensors8030067.
16. Sik M, Young M, Mirzaei A, Kim H, Kim S, Baek S, Won D, Jin C, Hyoung K (2021) Selective, sensitive, and stable NO_2 gas sensor based on porous ZnO nanosheets. Appl Surf Sci 568. https://doi.org/10.1016/j.apsusc.2021.150910.
17. Ying S, Wang Y, Wu Z, Huang M, Dong L (2021) Highly-sensitive NO_2 gas sensors based on three-dimensional nanotube graphene and ZnO nanospheres nanocomposite at room temperature. Appl Surf Sci 566. https://doi.org/10.1016/j.apsusc.2021.150720.
18. Xia Y, Zhou L, Yang J, Du P, Xu L, Wang J (2020) Highly sensitive and fast optoelectronic room-temperature NO_2 gas sensor based on ZnO nanorod-assembled macro-/mesoporous film, ACS Appl Electr Mater 2. https://doi.org/10.1021/acsaelm.9b00810.
19. Ding J, Chen S, Han N, Shi Y, Hu P, Li H, Wang J (2020) Aerosol assisted chemical vapour deposition of nanostructured ZnO thin films for NO_2 and ethanol monitoring. Ceram Int 46. https://doi.org/10.1016/j.ceramint.2020.03.051.
20. Khan MI, Ali S, Alwadai N, Irfan M, Albalawi H, Almuqrin AH, Almoneef MM, Iqbal M (2022) Structural, electrical and optical properties of hetrostructured MoS_2/ZnO thin films for potential perovskite solar cells application. J Mater Res Technol 20. https://doi.org/10.1016/j.jmrt.2022.07.082.
21. Chou CC, Shih LH, Chang SJ (2020) The study of humidity sensor based on Li-doped ZnO nanorods by hydrothermal method. Microsyst Technol 28. https://doi.org/10.1007/s00542-020-04957-9.
22. Saaédi A,Yousefi R (2017) Improvement of gas-sensing performance of ZnO nanorods by group-I elements doping. J Appl Phys 122. https://doi.org/10.1063/1.5009249.
23. Jasmi KK, Johny TA, Siril VS, Kumar V, Madhusoodanan KN (2022) Influence of defect chemistry on NO_2 gas sensing of Li-ZnO thin films. Bull Mater Sci 45. https://doi.org/10.1007/s12034-022-02798-y.
24. Shen H, Zhao X, Duan L, Liu R, Li H, Wang B (2017) Effect of Na_{Zn}/Na_i ratio on structural, optical, and electrical properties of Na-doped ZnO thin films, J Appl Phys 121. https://doi.org/10.1063/1.4980172.
25. Park CH, Zhang SB, Wei S (2002) Origin of p -type doping difficulty in ZnO: The impurity perspective. PhysRevB 66. https://doi.org/10.1103/PhysRevB.66.073202.
26. Akcan D, Gungor A, Arda L (2018) Structural and optical properties of Na-doped ZnO films. J Mol Struct 1161. https://doi.org/10.1016/j.molstruc.2018.02.058.
27. Erdogan NH, Kutlu T, Sedefoglu N, Kavak H (2021) Effect of Na doping on microstructures, optical and electrical properties of ZnO thin films grown by sol-gel method. J Alloys Compd 881. https://doi.org/10.1016/j.jallcom.2021.160554.
28. Chelouche A, Touam T, Boudjouan F, Djouadi D, Mahiou R, Bouloufa A, Chadeyron G., Hadjoub Z. (2017) Na doping effects on the structural, conduction type and optical properties of sol–gel ZnO thin films, J Mater Sci Mater Electron 28. https://doi.org/10.1007/s10854-016-5694-8.
29. Parmar NS, Yim H, Choi J (2017) Critical increase in Na-doping facilitates acceptor band movements that yields ~ 180 meV shallow hole conduction in ZnO bulk crystals. Nat Publ Gr 7. https://doi.org/10.1038/srep44196.

30. Mariappan R, Ponnuswamy V, Suresh R, Suresh P, Chandra Bose A, Ragavendar M (2014) Role of substrate temperature on the properties of Na-doped ZnO thin film nanorods and performance of ammonia gas sensors using nebulizer spray pyrolysis technique. J Alloys Compd 582. https://doi.org/10.1016/j.jallcom.2013.08.048.
31. Zhang L, Guo YY, Liu G, Tan Q (2020) Na-doped ZnO and RGO composite-based flexible acetone gas sensor operated in room temperature. IEEE Access 8. https://doi.org/10.1109/ACCESS.2020.3023028.
32. Johny TA, Kumar V, Imai H, Kanno I (2012) Influence of lithium doping on the structural and electrical characteristics of ZnO thin films. Thin Solid Films 520. https://doi.org/10.1016/j.tsf.2012.04.036.
33. Nisha R PhD Thesis (Cochin University of Science and Technology, India) (2013).
34. Kaur M, Shaheera M, Pathak A, Gadkari SC, Debnath AK (2021) Highly sensitive NO_2 sensor based on ZnO nanostructured thin film prepared by SILAR technique. Sens Actuators B Chem 335. https://doi.org/10.1016/j.snb.2021.129678.
35. Basyooni MA, Shaban M, El Sayed AM (2017) Enhanced gas sensing properties of spin-coated Na-doped ZnO nanostructured films. Nat Publ Gr 7. https://doi.org/10.1038/srep41716.
36. Akcan D, Gungor A, Arda L (2018) Structural and optical properties of Na-doped ZnO films. J Mol Struct 1161. https://doi.org/10.1016/j.molstruc.2018.02.058.
37. Elsayed MH, Elmorsi TM, Abuelela AM, Hassan AE, Alhakemy AZ, Bakr MF, et al. (2020) Direct sunlight-active Na-doped ZnO photocatalyst for the mineralization of organic pollutants at different pH mediums. J Taiwan Inst Chem Eng 115. https://doi.org/10.1016/j.jtice.2020.10.018.
38. Ye Z, Wang T, Wu S, Ji X, Zhang Q (2017) Na-doped ZnO nanorods fabricated by chemical vapor deposition and their optoelectrical properties, J Alloys Compd 690. https://doi.org/10.1016/j.jallcom.2016.08.100.
39. Ardyanian M, Sedigh N (2014) Heavy lithium-doped ZnO thin films prepared by spray pyrolysis method. Bull Mater Sci 37. https://doi.org/10.1007/s12034-014-0076-4.
40. Lü J, Huang K, Zhu J, Chen X, Song X, Sun Z (2010) Preparation and characterization of Na-doped ZnO thin films by sol-gel method, Phys B Condens Matter 405. https://doi.org/10.1016/j.physb.2010.04.045.
41. El Khalidi Z, Hartiti B, Siadat M, Comini E, Arachchige H.M.M.M., Fadili S, et al. (2019) Acetone sensor based on Ni doped ZnO nanostructues: growth and sensing capability, J Mater Sci Mater Electron 30. https://doi.org/10.1007/s10854-019-01083-9.
42. Patil VL, Vanalakar SA, Kamble AS, Shendage SS, Kim JH, Patil PS (2016) Farming of maize-like zinc oxide via a modified SILAR technique as a selective and sensitive nitrogen dioxide gas sensor. RSC Adv 6. https://doi.org/10.1039/C6RA06346B.
43. Khalid NR, Hammad A, Tahir MB, Rafique M, Iqbal T, Nabi G, Hussain MK Enhanced photocatalytic activity of Al and Fe co-doped ZnO nanorods for methylene blue degradation. Ceram Int 2019, 45. https://doi.org/10.1016/j.ceramint.2019.07.132.
44. Lawrence CJ (1988) The mechanics of spin coating of polymer films. Phys Fluids 31. https://doi.org/10.1063/1.866986.
45. Yan Y, Li J, Liu Q, Zhou P (2021) Evaporation effect on thickness distribution for spin-coated films on rectangular and circular substrates. Coatings, 11. https://doi.org/10.3390/coatings11111322.
46. Kumar RR, Murugesan T, Dash A, Hsu CH, Gupta S, Manikandan A, et al. (2021) Ultrasensitive and light-activated NO_2 gas sensor based on networked MoS2/ZnO nanohybrid with adsorption/desorption kinetics study. Appl Surf Sci 536. https://doi.org/10.1016/j.apsusc.2020.147933.
47. Ganesh RS, Durgadevi E, Navaneethan M, Patil VL, Ponnusamy S, Muthamizhchelvan C, Kawasaki S, Patil PS, Hayakawa Y (2018) Tuning the selectivity of NH3 gas sensing response using Cu-doped ZnO nanostructures, Sens Actuators A Phys 269. https://doi.org/10.1016/j.sna.2017.11.042.
48. Zhang YH, Li YL, Gong FL, Xie KF, Liu M, Zhang HL, Fang SM (2020) Al doped narcissus-like ZnO for enhanced NO_2 sensing performance: an experimental and DFT investigation. Sens Actuators B Chem 305. https://doi.org/10.1016/j.snb.2019.127489.
49. Kusumam TA, Siril VS, Madhusoodanan KN, Prashantkumar M, Ravikiran YT, Renuka NK (2020) NO_2 gas sensing performance of zinc oxide nanostructures synthesized by surfactant assisted Low temperature hydrothermal technique. Sens Actuators A Phys 318. https://doi.org/10.1016/j.sna.2020.112389.
50. Kwon YJ, Kang SY, Mirzaei A, Choi MS, Bang JH, Kim SS, Kim HW (2017) Enhancement of gas sensing properties by the functionalization of ZnO-branched SnO_2 nanowires with Cr_2O_3 nanoparticles, Sens Actuators B Chem 249. https://doi.org/10.1016/j.snb.2017.04.053.
51. Jin C, Park S, Kim H, Lee C (2012) Ultrasensitive multiple networked Ga_2O_3 -core / ZnO-shell nanorod gas sensors, Sens Actuators B Chem 161. https://doi.org/10.1016/j.snb.2011.10.023.
52. Kruefu V, Liewhiran C, Wisitsoraat A, Phanichphant S (2011) Selectivity of flame-spray-made Nb/ZnO thick films towards NO_2 gas, Sens Actuators B Chem 156. https://doi.org/10.1016/j.snb.2011.04.046.
53. Dİltemİz SE, Ecevİt K (2019) High-performance formaldehyde adsorption on CuO / ZnO composite nano fi ber coated QCM sensors. J Alloys Compd 783. https://doi.org/10.1016/j.jallcom.2018.12.237.
54. Kwon YJ, Mirzaei A, Kang SY, Choi MS, Bang JH, Kim SS, Kim HW (2017) Synthesis, characterization and gas sensing properties of ZnO-decorated MWCNTs. Appl Surf Sci 413. https://doi.org/10.1016/j.apsusc.2017.03.290.
55. Sanger A, Kang SB, Jeong MH, Kim CU, Baik JM, Choi KJ (2019) All-transparent NO_2 gas sensors based on freestanding Al-doped ZnO nanofibers. ACS Appl Electron Mater 1. https://doi.org/10.1021/acsaelm.9b00210.